Title
Anomalous Self-Assembly and Ion Transport in Nanostructured Organic–Inorganic Solid Electrolytes

Journal
ACS Macro Letters, 7(9)

ISSN
2161-1653

Authors
Sethi, Gurmukh K
Jiang, Xi
Chakraborty, Rohan
et al.

Publication Date
2018-09-18

DOI
10.1021/acsmacrolett.8b00583

Peer reviewed

Anomalous self-assembly and ion transport in nanostructured organic-inorganic solid electrolytes

Gurmukh K. Sethi[†, ‡], Xi Jiang[‡], Rohan Chakraborty[∥], Whitney S. Loo[∥], Irune Villaluenga[‡,§,*], and Nitash P. Balsara[‡,∥,§,⊥,*]

[†]Department of Materials Science and Engineering and [∥]Department of Chemical and Biomolecular Engineering, University of California, Berkeley, California 94720, USA

[‡]Materials Science Division, [§]Joint Center for Energy Storage Research (JCESR), and [⊥]Energy Storage and Distributed Resources Division, Lawrence Berkeley National Laboratory, Berkeley, California 94720, USA

ABSTRACT: Nanostructured solid electrolytes containing ion-conducting domains and rigid non-conducting domains are obtained by block copolymer self-assembly. Here, we report on the synthesis and characteristics of mixtures of a hybrid diblock copolymer with an organic and inorganic block: poly(ethylene oxide) -*b*- poly(acryloisobutyl polyhedral oligomeric silsesquioxane) (PEO-POSS) and a lithium salt. In the neat state, PEO-POSS exhibits a classical order-to-disorder transition upon heating. Dilute electrolytes exhibit a dramatic reversal; a disorder-to-order transition upon heating is obtained, indicating that the addition of salt fundamentally changes interactions between the organic and inorganic chains. At higher salt concentrations, the electrolytes primarily form a lamellar phase. Coexisting lamellae and cylinders are found at intermediate salt concentrations and high temperatures. The conductivity and shear modulus of PEO-POSS are significantly higher than that of an all-organic block copolymer electrolyte with similar molecular weight and morphology, demonstrating that organic-inorganic block copolymers provide a promising route for developing the next generation of solid electrolytes for lithium batteries.

Polymer electrolytes offer increased stability in lithium batteries in comparison to more widely used liquid electrolytes[1–4]. Nanostructured electrolytes containing both soft, ion-conducting domains and rigid non-conducting domains offer the opportunity to tune both mechanical and electrical properties separately. Such electrolytes are conveniently made by block copolymer self-assembly[5–7]. Most of the block copolymer electrolytes studied thus far comprise organic polymer chains for both the conducting and rigid domains. Nanostructured hybrid materials are often made via block copolymer self-assembly, either using the domain structure of block copolymers as a template for synthesizing confined inorganic domains or by attaching molecular structures such as polyhedral oligomeric silsesquioxane (POSS) to a polymerizable monomer unit[8–19]. While such nanocomposites have been studied extensively, we are not aware of any quantification of the thermodynamic interactions between polymers wherein one of the components contains an inorganic moiety. A fundamental understanding of self-assembly in such systems begins with the quantification of these interactions.

In this paper we report on the synthesis and characterization of a poly(ethylene oxide) -*b*- poly(acryloisobutyl polyhedral oligomeric silsesquioxane) (PEO-POSS) diblock copolymer. The block copolymer was synthesized by nitroxide-mediated radical polymerization of a POSS containing monomer (acryloisobutyl POSS) using functionalized PEO as the macroinitiator. Our synthetic procedure is given in the Supporting Information and the chemical structure of PEO-POSS is shown in Figure 1a. PEO and POSS blocks are 5 kg mol^{-1} and 1.9 kg mol^{-1} respectively. The density of PEO and POSS homopolymers at 120 °C was measured to be 1.05 and 1.30 g cm^{-3} as described in the Supporting Information. The volume fraction, $\phi_{EO,}$ of the POSS block based on these measurements is 0.23. Electrolytes were prepared by mixing lithium bis(trifluoromethane)sulfonimide (LiTFSI) salt into the block copolymer.

Small angle x-ray scattering (SAXS) profiles of neat PEO-POSS at selected temperatures between 85 °C and 132 °C (both blocks are amorphous in this temperature range) are shown in Figure 1b where scattering intensity, I, is plotted as a function of the magnitude of the scattering vector, q. At 85 °C we obtain a primary

scattering peak at $q = q^* = 0.32$ nm^{-1} and a second order scattering peak at $2q^*$. This is a standard signature of a lamellar phase. The center-to-center distance between adjacent PEO lamellae, d, given by $d = 2\pi/q^*$, is 19.6 nm. This morphology persists until 122 °C. At 127 °C, the intensity of the primary scattering peak diminishes significantly and the second order peak disappears. This SAXS profile indicates the presence of disordered concentration fluctuations. It is evident that neat PEO-POSS exhibits an order-to-disorder transition upon heating at 125 ±

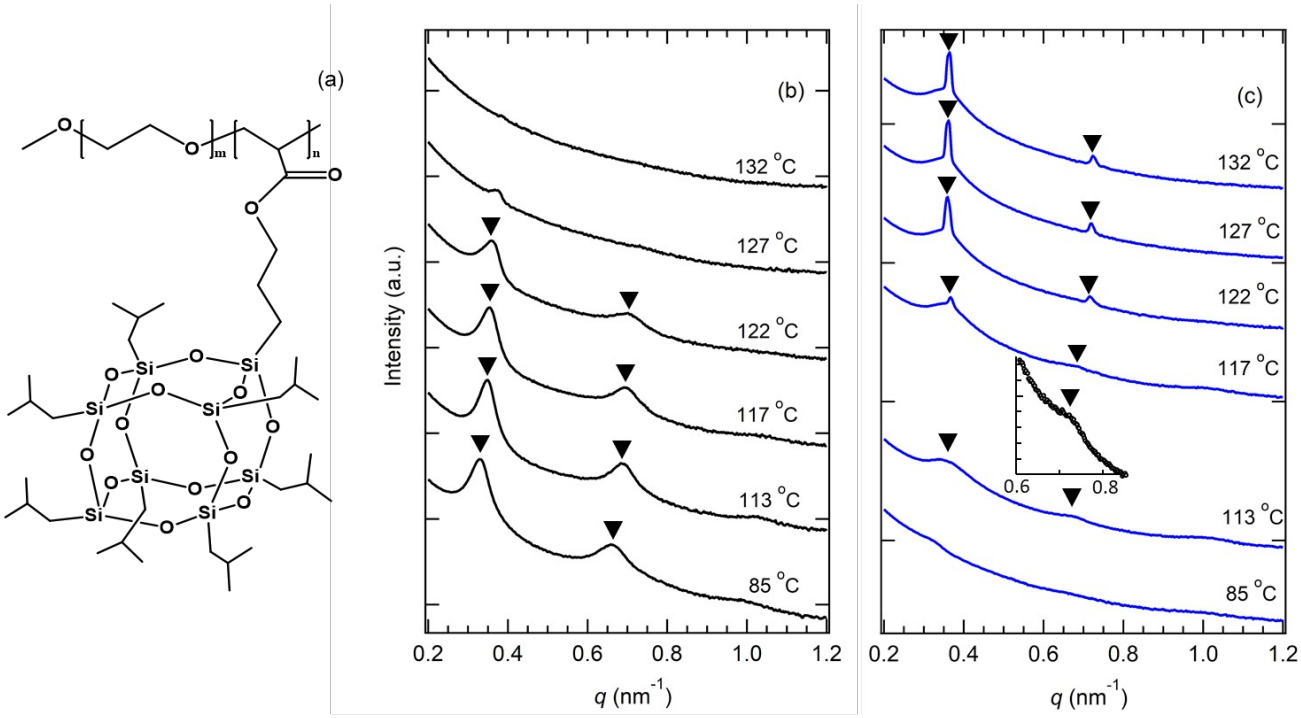

Figure 1. (a) The chemical structure of PEO-POSS. Scattering intensity of PEO-POSS at selected temperatures, plotted as a function of the magnitude of the scattering vector, q (b) neat polymer and (c) PEO-POSS/LiTFSI mixture at $r = 0.02$. Profiles are shifted vertically. Triangles indicate peaks at q^* and $2q^*$ that signify lamellar order.

3 °C. This behavior, that is qualitatively similar to that of most organic block copolymers, suggests that PEO and POSS chains exhibit repulsive interactions[20–22]. At low temperatures, these interactions dominate, leading to an ordered phase. At high temperatures entropic effects dominate, leading to mixing of PEO and POSS segments. The estimated Flory Huggins interaction parameter, based on a reference volume of 0.1 nm^3, at 125 °C is 0.18 using a diblock copolymer phase diagram developed in ref 23 (see Supporting Information).

The SAXS profiles obtained from a PEO-POSS/LiTFSI mixture with $r = 0.02$ are shown in Figure 1c. At 85 °C, I is a monotonically decaying function of q, qualitatively similar to the 132 °C data obtained from neat PEO-POSS. We therefore conclude that the $r = 0.02$ sample is disordered at this temperature. Increasing the temperature to 113 °C results in broad SAXS peaks at $q = q^* = 0.33$ nm^{-1} and at $q = 2q^*$; see inset in Figure 1c. The emergence of the higher order peak is taken to be a signature of the disorder-to-order transition. (There is a hint of a broad peak at $q = 3q^*$ in the 113 °C data in Figure 1c). Disorder-to-order transitions upon heating have been reported in several neat diblock copolymer systems[24–30]. Increasing the temperature further to 117 °C results in the appearance of sharp peaks at $q = q^* = 0.35$ nm^{-1} and at $2q^*$. The SAXS profile at 122 °C and above are characteristic of a well-ordered lamellar phase. The scattering peaks obtained from the lamellar phase at $r = 0.02$ are significantly sharper than those seen in the neat copolymer (compare the 85 °C scattering profile in Figure 1b with 132 °C scattering profile in Figure 1c). This observation indicates that the high temperature ordered phase obtained in

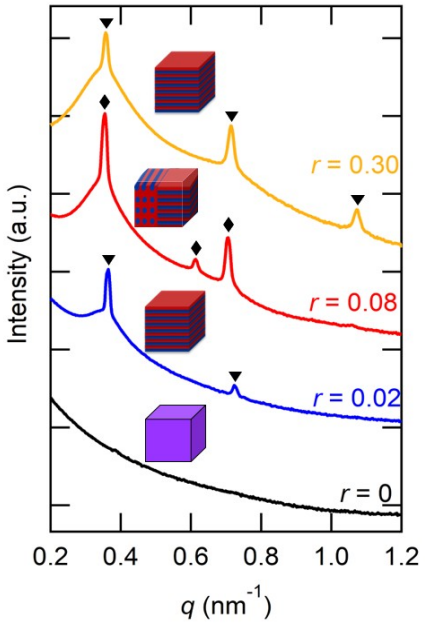

Figure 2. Scattering intensity of PEO-POSS/LiTFSI mixtures at 132 °C is plotted as a function of the magnitude of the scattering vector, q. The salt concentration of each profile is indicated on the right. Profiles are shifted vertically. Triangles indicate peaks due to lamellar order (q^*, $2q^*$) and diamonds indicate peaks due to cylindrical order (q^*, $\sqrt{3}q^*$,$2q^*$). The morphology is indicated by the diagrams in the center.

the salt-containing PEO-POSS sample exhibits better long-range order than the low temperature ordered phase in neat PEO-POSS. Whether this is due to the presence of salt or the annealing of defects at higher temperature is unclear at this juncture. The primary scattering peak at 117 °C appears to be a superposition of the broad peak seen at 113 °C and the sharp peak seen at 122 °C. The superposition may also be due to the presence of two coexisting ordered phases with different salt concentrations[31].

It is well known that if salt interacts exclusively with the PEO block, one observes stabilization of the ordered phase[32–38]. In contrast, in salt-containing PEO-POSS at temperatures below 97 °C the addition of salt stabilizes the disordered phase. The data in Figure 1 suggests that the salt molecules interact with both PEO and POSS segments. While further work is needed to identify the nature of these interactions, they are strong enough to cause mixing between chains that are immiscible without salt. At sufficiently high temperatures, entropic contributions dominate, the relative importance of specific interactions diminishes, and PEO and POSS segments form separate domains.

The effect of added salt on the morphology of PEO-POSS electrolytes is shown in Figure 2 for a range of salt concentrations at 132 °C. The neat sample is disordered at this temperature, while all salt containing samples are ordered. At low salt concentration, r = 0.02, a lamellar phase is obtained. Increasing the salt concentration to r = 0.08 results in the emergence of an additional scattering peak at $q = \sqrt{3}q^*$ that is superimposed on the scattering profile of the lamellar phase. This peak is a signature of a hexagonally packed cylinders morphology. Increasing salt concentration further to r = 0.30 results in a reentrant lamellar phase. The dependence of domain spacing on salt concentration and temperature is shown in the Supporting Information.

Figure 3 summarizes the results of the SAXS experiments, where the morphologies of PEO-POSS/LiTFSI mixtures are shown as a function of temperature and salt concentration. The lamellar (L) phase dominates the phase diagram which contains isolated pockets of disordered (D) and coexisting cylinders/lamellae (C/L). This is surprising given ϕ_{EO} is 0.77. Determining the distribution of salt in the two coexisting microphases is beyond the scope of this study. Using the assumption that is standard in the field of block copolymer electrolytes that LiTFSI resides exclusively in the PEO domains[35,39,40], the estimated volume fraction of the PEO-rich phase increases with salt addition to ϕ_{EO} = 0.86 at r = 0.30. This estimated volume fraction is shown as the secondary (top) x-axis in Figure 3. The geometry of ordered phases in conventional block copolymers depends mainly on the volume fraction of one of the blocks[41,42]. Increasing the volume fraction of the major component is expected to stabilize either cylinders or spheres, not lamellae[22,43]. If this were true in PEO-POSS, cylinders would emerge at high salt concentration. Clearly, this is not the case. The sample with ϕ_{EO} = 0.86 exhibits a lamellar morphology over the entire accessible temperature window. Cylinders are only seen at high temperatures in a limited window ($0.06 \leq r \leq 0.1$). We posit that the specific interactions between salt, PEO, and POSS that stabilize the disordered phase in the dilute electrolyte are also responsible for the unexpected stabilization of the lamellar phase. At high temperatures, the importance of these interactions diminishes, leading to the formation of the expected cylinder phase. We note that the Gibbs phase rule requires coexistence at all phase boundaries in Figure 3. This suggests the presence of a pure cylinder phase at temperatures above 132 °C.

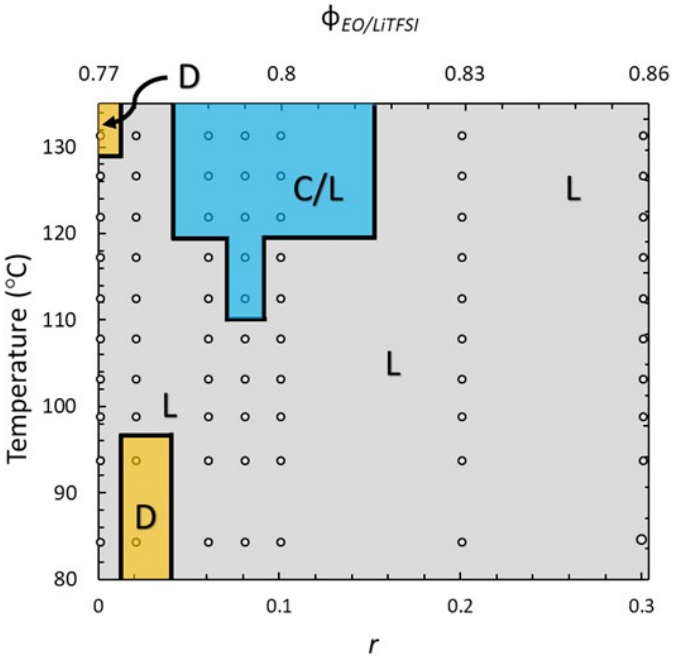

Figure 3. Morphology of phases on a temperature versus salt concentration (r) plot: lamellar (L), disordered (D), and hexagonally packed cylinders (C) which always coexist with lamellae. The top axis is volume fraction of the EO/LiTFSI-rich phase.

Electron microscopy was used to elucidate the nature of the ordered phases reported in Figure 4. Two samples of the r = 0.08 electrolyte were annealed at 94 °C and 130 °C and quenched in liquid nitrogen to “freeze” the morphology at these temperatures. The resulting micrographs, obtained by high-angle annular dark-field scanning transmission electron microscopy (HAADF-STEM) are shown in Figure 4b and Figure 4c where the bright phase represents the RuO_4 stained PEO-rich microphases. The micrograph obtained from the 94 °C sample shows alternating dark and bright stripes representing the lamellar phase. The micrograph obtained from the 130 °C sample shows both dark spots arranged on a hexagonal lattice (Figure 4c inset), confirming the presence of POSS-rich cylinders in a PEO-rich matrix, and alternating POSS-rich and PEO-rich stripes.

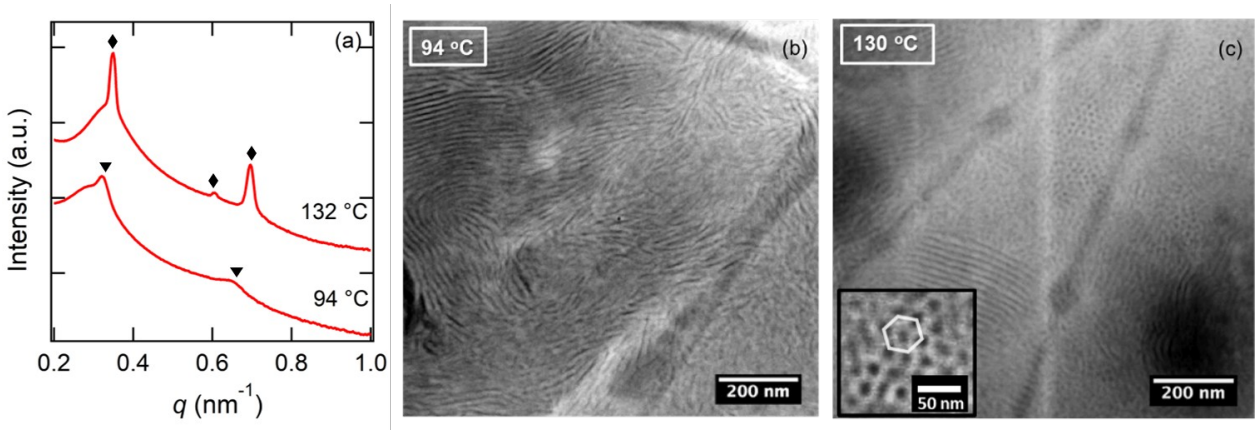

Figure 4. (a) SAXS scattering profiles are taken at 94 °C, with scattering peaks indicative of a lamellar morphology indicated by triangles, and 132 °C with scattering peaks denoted by diamonds indicating coexisting cylinders and lamellae. (b) and (c) HAADF-STEM micrographs of RuO_4-stained PEO-POSS electrolytes with r = 0.08. The bright phase represents the RuO_4-stained PEO-rich phase. Separate samples were annealed at selected temperatures and quenched using liquid nitrogen. (b) Sample annealed at 94 °C showing lamellar morphology. (c) Sample annealed at 130 °C showing coexisting hexagonally packed cylinders and lamellae. SAXS and TEM data are consistent with each other.

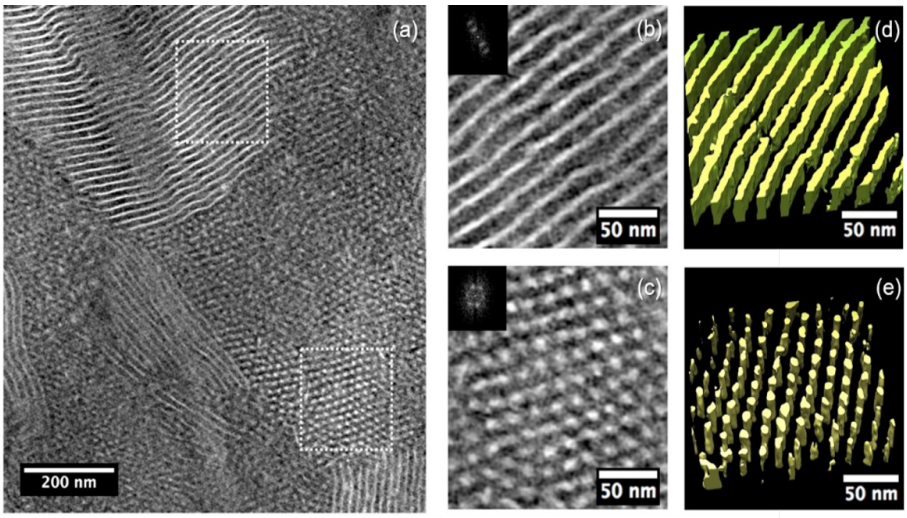

Figure 5. Electron Tomography of PEO-POSS r = 0.08 showing coexisting lamellae and cylinders. Sample was quenched in liquid nitrogen after annealing at 130 °C and the scans were taken at room temperature. (a) Bright field tomogram where the dark phase represents the stained EO-rich microphase. (b) and (c) Boxed regions shown on an expanded scale. Insets show Fourier transforms of the images. (d) 3-D tomogram of (b) showing a lamellar phase. (e) 3-D tomogram of (c) showing hexagonally packed cylinders.

To confirm that the stripes seen in Figure 4c correspond to a lamellar phase as opposed to cylinders lying in the sample plane, electron tomography of the r = 0.08 electrolyte annealed at 130 °C was utilized, and the results are shown in Figure 5. Figure 5a shows a slice of the tomogram where POSS is the bright phase and PEO is the dark phase. Bright spots arranged in a hexagonal lattice imply POSS rich-cylinders and alternating bright and dark stripes indicate lamellae. Figures 5b and 5c are magnifications of the outlined boxes in Figure 5a that depict the lamellar and cylindrical morphology, respectively. Fourier transforms of the real-space images are also provided to confirm these lattice arrangements. Figure 5d is a 3D representation of the POSS-rich phase of the tomogram shown in Figure 5b. It indicates the presence of lamellae. Similarly, Figure 5e, which is a 3D representation of Figure 5c, shows the presence of POSS-rich cylinders. Thus, the coexistence of lamellae and cylinders is confirmed by both SAXS and electron tomography.

The transport of lithium ions in polymers is facilitated by the segmental motion which is rapid in soft polymers such as amorphous PEO[47]. The goal of creating block copolymer electrolytes is to increase the modulus of the electrolyte while minimizing the decrease in ionic conductivity due to the presence of non-conducting domains. The ionic conductivity of PEO-POSS electrolytes is plotted as a function of salt concentration at 90 °C in Figure 6a. The electrolytes have a lamellar morphology at all values of r except r = 0.02,

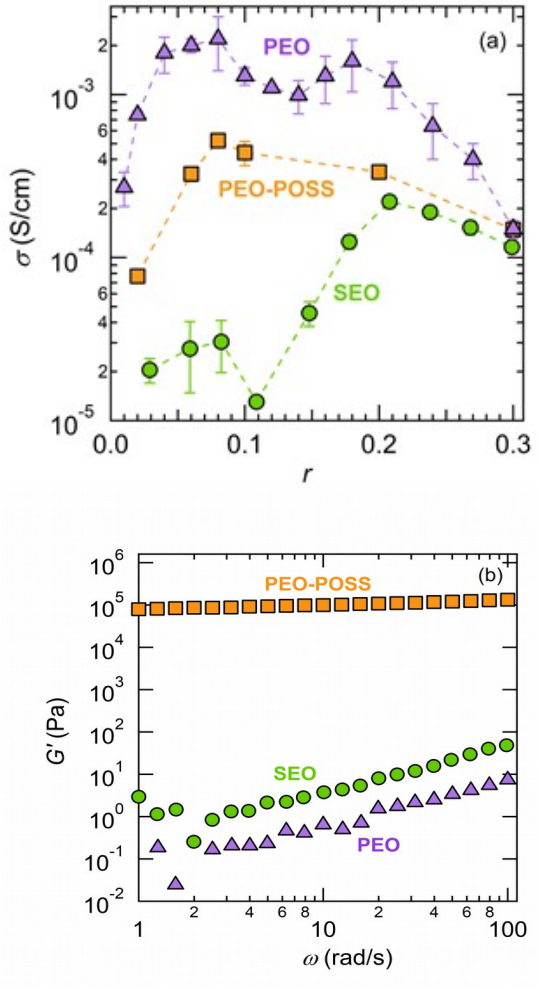

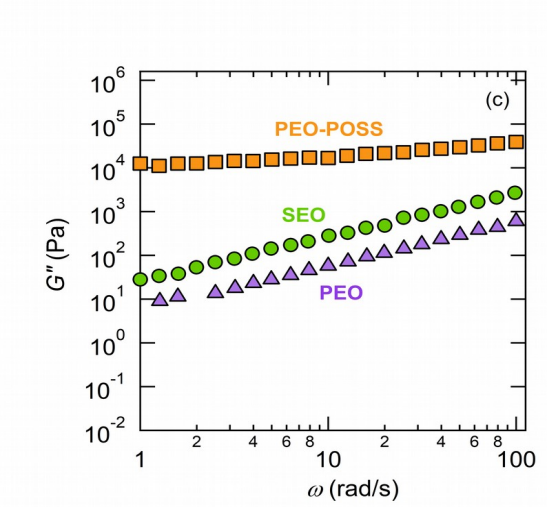

Figure 6. Dependence of ionic conductivity on salt concentration and rheological properties of neat polymers at 90 °C. (a) Ionic conductivity, σ, is plotted against salt concentration, *r*, for the block copolymers PEO-POSS, SEO[44], and homopolymer PEO[45]. (b) and (c) Storage and loss shear moduli, G′ and G″, plotted against frequency, *ω,* for PEO-POSS, SEO[46], and homopolymer PEO[46].

where it forms a disordered phase. Also shown in Figure 6a is the conductivity of homopolymer PEO electrolyte with a molecular weight of 5 kg mol^{-1} and that of a conventional polystyrene-*b*-poly(ethylene oxide) (SEO) electrolyte with molecular weights of 5 kg mol^{-1} of both blocks (ϕ_{EO} = 0.52)[32]. We chose this SEO copolymer because it has the same molecular weight for the conducting block and exhibits a lamellar morphology[44]. Both SEO and PEO-POSS electrolytes exhibit lower conductivities than PEO electrolyte, as expected. However, in the dilute limit, the conductivity of PEO-POSS electrolytes are much higher than that of SEO, by factors ranging from 2 to 10.

The rheological properties of PEO-POSS, PEO (20 kg mol^{-1}), and SEO are shown in Figure 6b and 6c at 90 °C. (The modulus of PEO (5 kg mol^{-1}) was below the dynamic range
of our rheological instrument.) We only present data obtained from the neat polymers due to the hygroscopic nature of the salt-containing electrolytes. The low frequency storage modulus (G′) of SEO is about a factor of 10 higher than PEO, while the loss modulus (G") is about a factor of 5 higher. Both G′ and G″ of SEO and PEO decrease rapidly with decreasing frequency. In contrast, G′ of PEO-POSS is nearly independent of frequency while G″ decreases slightly in the frequency range studied. The G′ of PEO-POSS at low frequency (ω = 1 rad/s) is a factor of 10^5 higher than SEO, while G″ is over a factor of 10^2 higher than SEO.

In summary, PEO-POSS represents a new platform for creating self-assembled hybrid electrolytes for lithium batteries. In the absence of salt, PEO-POSS presents a classical order-to-disorder transition upon heating. The addition of salt at low concentration results in a disorder-to-order transition upon heating. Further increase in salt concentration results in the stabilization of ordered phases. In conventional block copolymers, spherical or cylindrical morphologies are expected when the volume fraction of the major phase is between 0.77 and 0.86. In PEO-POSS, we primarily obtain lamellar phases. The cylindrical morphology is only stable at high temperatures and intermediate salt concentrations. The ionic conductivity of lamellar PEO-POSS electrolytes is higher than that of SEO at all salt concentrations at 90 °C; at *r* = 0.10 the conductivity of PEO-POSS is 50 times higher than that of SEO. The low frequency G′ of PEO-POSS is five orders of magnitude higher than that of SEO. Further work on optimizing the properties of organic-inorganic hybrid block copolymers for use in all-solid lithium batteries seems warranted.

ASSOCIATED CONTENT

Supporting Information. Experimental techniques and results. This material is available free of charge via the Internet at http://pubs.acs.org.

AUTHOR INFORMATION

Corresponding Authors

nbalsara@berkeley.edu
iruneuskal@gmail.com

Author Contributions

The manuscript was written through contributions of all authors. All authors have given approval to the final version of the manuscript.

ACKNOWLEDGMENT

This work was supported as part of the Joint Center for Energy Storage Research, an Energy Innovation Hub funded by the U.S. Department of Energy, Office of Science, Basic Energy Sciences. Funding for the electron tomography work was provided by the Soft Matter Electron Microscopy Program, supported by the Office of Science, Office of Basic Energy Science, U.S. Department of Energy, under Contract No. DE-AC02-05CH11231. The electron microscopy work was performed at Donner Lab, and the x-ray work was performed at Advanced Light Source, which is a DOE Office of Science User Facility, was supported by Contract No. DE-AC02- 05CH11231. Work at the Stanford Synchrotron Radiation Light Source, a user facility at SLAC National Accelerator Laboratory, was supported by the U.S. Department of Energy, Office of Science, Office of Basic Energy Sciences under Contract No. DE-AC02-76SF00515.

G.K.S. acknowledges funding from a National Science Foundation Graduate Student Research Fellowship.

REFERENCES

(1) Fenton, D. E., Parker, J. M. & Wright, P. V. Complexes of alkali metal ions with poly(ethylene oxide). *Polymer (Guildf).* **14,** 589 (1973).

(2) Berthier, C., Gorecki, W., Minier, M., Armand, M. B., Chabagno, J. M. & Rigaud, P. Microscopic investigation of ionic conductivity in alkali metal salts-poly(ethylene oxide) adducts. *Solid State Ionics* **11,** 91–95 (1983).

(3) Bouchet, R., Maria, S., Meziane, R., Aboulaich, A., Lienafa, L., Bonnet, J. P., Phan, T. N. T., Bertin, D., Gigmes, D., Devaux, D., Denoyel, R. & Armand, M. Single-ion BAB triblock copolymers as highly efficient electrolytes for lithium-metal batteries. *Nat. Mater.* **12,** 452–457 (2013).

(4) Armand, M. & Tarascon, J. M. Building better batteries. *Nature* **451,** 652–657 (2008).

(5) Devaux, D., Glé, D., Phan, T. N. T., Gigmes, D., Giroud, E., Deschamps, M., Denoyel, R. & Bouchet, R. Optimization of Block Copolymer Electrolytes for Lithium Metal Batteries. *Chem. Mater.* **27,** 4682–4692 (2015).

(6) Croce, F., Appetecchi, G. B., Persi, L. & Scrosati, B. Nanocomposite polymer electrolytes for lithium batteries. *Nature* **394,** 456–458 (1998).

(7) Sing, C. E., Zwanikken, J. W. & Olvera De La Cruz, M. Electrostatic control of block copolymer morphology. *Nat. Mater.* **13,** 694–698 (2014).

(8) Hirai, T., Leolukman, M., Liu, C. C., Han, E., Kim, Y. J., Ishida, Y., Hayakawa, T., Kakimoto, M. A., Nealey, P. F. & Gopalan, P. One-step direct-patterning template utilizing self-assembly of POSS-containing block copolymers. *Adv. Mater.* **21,** 4334–4338 (2009).

(9) Misner, M. J., Skaff, H., Emrick, T. & Russell, T. P. Directed deposition of nanoparticles using diblock copolymer templates. *Adv. Mater.* **15,** 221–224 (2003).

(10) Sohn, B. H. & Cohen, R. E. Silver nanocluster formation within microphase-separated block copolymers. *Acta Polym.* **47,** 340–343 (1996).

(11) Zhang, J., Ma, C., Liu, J., Chen, L., Pan, A. & Wei, W. Solid polymer electrolyte membranes based on organic/inorganic nanocomposites with star-shaped structure for high performance lithium ion battery. *J. Memb. Sci.* **509,** 138–148 (2016).

(12) Goseki, R., Hirai, T., Ishida, Y., Kakimoto, M. A. & Hayakawa, T. Rapid and reversible morphology control in thin films of poly(ethylene oxide)-block-POSS-containing poly(methacrylate). *Polym. J.* **44,** 658–664 (2012).

(13) Kim, S. K., Kim, D. G., Lee, A., Sohn, H. S., Wie, J. J., Nguyen, N. A., MacKay, M. E. & Lee, J. C. Organic/inorganic hybrid block copolymer electrolytes with nanoscale ion-conducting channels for lithium ion batteries. *Macromolecules* **45,** 9347–9356 (2012).

(14) Daga, V. K., Anderson, E. R., Gido, S. P. & Watkins, J. J. Hydrogen Bond Assisted Assembly of Well-Ordered Polyhedral Oligomeric SilsesquioxaneÀBlock Copolymer Composites. 6793–6799 (2011). doi:10.1021/ma200926n

(15) Romo-Uribe, A. Viscoelastic Behavior of Unentangled POSS–Styrene Nanocomposites and the Modification of Macromolecular Dynamics. *Macromolecules* acs.macromol.7b01645 (2017). doi:10.1021/acs.macromol.7b01645

(16) Ayandele, E., Sarkar, B. & Alexandridis, P. Polyhedral Oligomeric Silsesquioxane (POSS)-Containing Polymer Nanocomposites. *Nanomaterials* **2,** 445–475 (2012).

(17) Polu, A. R. & Rhee, H. W. Nanocomposite solid polymer electrolytes based on poly(ethylene oxide)/POSS-PEG (n=13.3) hybrid nanoparticles for lithium ion batteries. *J. Ind. Eng. Chem.* **31,** 323–329 (2015).

(18) Lee, J. Y., Lee, Y. M., Bhattacharya, B., Nho, Y. C. & Park, J. K. Solid polymer electrolytes based on crosslinkable polyoctahedral silsesquioxanes (POSS) for room temperature lithium polymer batteries. *J. Solid State Electrochem.* **14,** 1445–1449 (2010).

(19) Wang, D. K., Varanasi, S., Strounina, E., Hill, D. J. T., Symons, A. L., Whittaker, A. K. & Rasoul, F. Synthesis and characterization of a POSS-PEG macromonomer and POSS-PEG-PLA hydrogels for periodontal applications. *Biomacromolecules* **15,** 666–679 (2014).

(20) Sakamoto, N. & Hashimoto, T. Order-Disorder Transition of Low Molecular Weight Polystyrene-block-Polyisoprene. 1. SAXS Analysis of Two Characteristic Temperatures. *Macromolecules* **28,** 6825–6834 (1995).

(21) Leibler, L. Theory of Microphase Separation in Block Copolymers. *Macromolecules* **13,** 1602–1617 (1980).

(22) Fredrickson, G. H. & Helfand, E. Fluctuation effects in the theory of microphase separation in block copolymers. *J. Chem. Phys.* **87,** 697–705 (1987).

(23) Cochran, E. W., Garcia-Cervera, C. J. & Fredrickson, G. H. Stability of the gyroid phase in diblock copolymers at strong segregation. *Macromolecules* **39,** 2449–2451 (2006).

(24) Russell, T. P., Karis, T. E., Gallot, Y. & Mayes, A. M. A lower critical ordering transition in a diblock copolymer melt. *Nature* **368,** 729–731 (1994).

(25) Ruzette, A.-V. G., Banerjee, P., Mayes, A. M., Pollard, M., Russell, T. P., Jerome, R., Slawecki, T., Hjelm, R. & Thiyagarajan, P. Phase Behavior of Diblock Copolymers between Styrene and *n* -Alkyl Methacrylates. *Macromolecules* **31,** 8509–8516 (1998).

(26) Haris, T. E., Russell, T. P., Gallot, Y. & Mayes, A. M. Rheology of the Lower Critical Ordering Transition. *Macromolecules* **28,** 1129–1134 (1995).

(27) Pollard, M., Russell, T. P., Ruzette, A. V., Mayes, A. M. & Gallot, Y. The effect of hydrostatic pressure on the lower critical ordering transition in diblock copolymers. *Macromolecules* **31,** 6493–6498 (1998).

(28) Ryu, D. Y., Shin, C., Cho, J., Lee, D. H., Kim, J. K., Lavery, K. A. & Russell, T. P. Effective interaction parameter for homologous series of deuterated polystyrene-block-poly(n-alkyl methacrylate) copolymers. *Macromolecules* **40,** 7644–7655 (2007).

(29) Yeh, C. L., Hou, T., Chen, H. L., Yeh, L. Y., Chiu, F. C., M??ller, A. J. & Hadjichristidis, N. Lower critical ordering transition of poly(ethylene oxide)-block-poly(2-vinylpyridine). *Macromolecules* **44,** 440–443 (2011).

(30) Mulhearn, W. D. & Register, R. A. Lower critical ordering transition of an all-hydrocarbon polynorbornene diblock copolymer. *ACS Macro Lett.* **6,** 808–812 (2017).

(31) Loo, W. S., Jiang, X., Maslyn, J. A., Oh, H. J., Zhu, C., Downing, K. H. & Balsara, N. P. Reentrant phase behavior and coexistence in asymmetric block copolymer electrolytes. *Soft Matter* (2018). doi:10.1039/C8SM00175H

(32) Teran, A. A. & Balsara, N. P. Thermodynamics of block copolymers with and without salt. *J. Phys. Chem. B* **118,** 4–17 (2014).
(33) Young, W. S. & Epps, T. H. Salt doping in PEO-containing block copolymers: Counterion and concentration effects. *Macromolecules* **42,** 2672–2678 (2009).
(34) Gunkel, I. & Thurn-Albrecht, T. Thermodynamic and structural changes in ion-containing symmetric diblock copolymers: A small-angle X-ray scattering study. *Macromolecules* **45,** 283–291 (2012).
(35) Nakamura, I. & Wang, Z.-G. Salt-doped block copolymers: ion distribution, domain spacing and effective χ parameter. *Soft Matter* **8,** 9356 (2012).
(36) Mai, S. M., Fairclough, J. P. A., Hamley, I. W., Matsen, M. W., Denny, R. C., Liao, B. X., Booth, C. & Ryan, A. J. Order-disorder transition in poly(oxyethylene)-poly(oxybutylene) diblock copolymers. *Macromolecules* **29,** 6212–6221 (1996).
(37) Qin, J. & De Pablo, J. J. Ordering Transition in Salt-Doped Diblock Copolymers. *Macromolecules* **49,** 3630–3638 (2016).
(38) Schulze, M. W., McIntosh, L. D., Hillmyer, M. A. & Lodge, T. P. High-modulus, high-conductivity nanostructured polymer electrolyte membranes via polymerization-induced phase separation. *Nano Lett.* **14,** 122–126 (2014).
(39) Gomez, E. D., Panday, A., Feng, E. H., Chen, V., Stone, G. M., Minor, A. M., Kisielowski, C., Downing, K. H., Borodin, O., Smith, G. D. & Balsara, N. P. Effect of ion distribution on conductivity of block copolymer electrolytes. *Nano Lett.* **9,** 1212–1216 (2009).
(40) Panday, A., Mullin, S., Gomez, E. D., Wanakule, N., Chen, V. L., Hexemer, A., Pople, J. & Balsara, N. P. Effect of molecular weight and salt concentration on conductivity of block copolymer electrolytes. *Macromolecules* **42,** 4632–4637 (2009).
(41) Almdal, K., koppi, K. A., Bates, F. S. & Mortensen, K. Multiple Ordered Phases in a Block Copolymer Melt. *Macromolecules* **25,** 1743–1751 (1992).
(42) Hasegawa, H., Tanaka, H., Yamasaki, K. & Hashimoto, T. Bicontinuous Microdomain Morphology of Block Copolymers: 1: Tetrapod-Network Structure of Polystyrene-Polyisoprene Diblock Polymers. *Macromolecules* **20,** 1651–1662 (1987).
(43) Bates, F. S. & Fredrickson, G. H. Block copolymers-designer soft materials. *Phys. Today* **52,** 32–38 (1999).
(44) Chintapalli, M., Le, T. N. P., Venkatesan, N. R., Mackay, N. G., Rojas, A. A., Thelen, J. L., Chen, X. C., Devaux, D. & Balsara, N. P. Structure and Ionic Conductivity of Polystyrene-block-poly(ethylene oxide) Electrolytes in the High Salt Concentration Limit. *Macromolecules* **49,** 1770–1780 (2016).
(45) Pesko, D. M., Timachova, K., Bhattacharya, R., Smith, M. C., Villaluenga, I., Newman, J. & Balsara, N. P. Negative Transference Numbers in Poly(ethylene oxide)-Based Electrolytes. *J. Electrochem. Soc.* **164,** E3569–E3575 (2017).
(46) Stone, G. M., Mullin, S. A., Teran, A. A., Hallinan, D. T., Minor, A. M., Hexemer, A. & Balsara, N. P. Resolution of the Modulus versus Adhesion Dilemma in Solid Polymer Electrolytes for Rechargeable Lithium Metal Batteries. *J. Electrochem. Soc.* **159,** A222–A227 (2012).
(47) Lascaud, S., Perrier, M., Vallée, A., Besner, S., Prud'homme, J. & Armand, M. Phase Diagrams and Conductivity Behavior of Poly(ethylene oxide)-Molten Salt Rubbery Electrolytes. *Macromolecules* **27,** 7469–7477 (1994).